Desalination and Water Treatment
www.deswater.com
doi: 10.5004/dwt.2021.26793

217 (2021) 203–213
March

Removal of molybdenum(VI) by nanoscale iron sulfide: kinetics and influence factors

Bo Chen[a], Fan-jie Zhou[a], Jian-jun Lian[a,*], Long-mian Wang[b], Ping Wang[a], Meng Wu[a], Tian-na Wang[a], Qing Xu[a]

[a]*College of Energy and Environment, Anhui University of Technology, Anhui 243002, China, emails: jjlian85@126.com (J.-j. Lian), greenchenbo@163.com (B. Chen), 1300154477@qq.com (F.-j. Zhou), 13449095@qq.com (P. Wang), 1723834029@qq.com (M. Wu), 3120493110@qq.com (T.-n. Wang), 1319987478@qq.com (Q. Xu)*
[b]*Nanjing Institute of Environmental Sciences, Ministry of Ecology and Environment, Nanjing 210042, China, email: wlmian@sina.com*

Received 12 June 2020; Accepted 16 November 2020

ABSTRACT

Iron sulfide (FeS) has attracted increasing interest as one of the most important reductants in anoxic environments towards various contaminants. However, some important factors influencing the removal of molybdenum (Mo) by FeS have not been studied clearly. The overall goal of this study was to investigate the effects of the kinetic process, initial pH, dissolved oxygen, co-existing ions, and temperature on Mo(VI) removal by FeS. Spectroscopic analyses demonstrate that Mo(VI) have been successfully reduced to Mo(IV-V) and immobilized on FeS at pH 4. The process of Mo(VI) immobilization on FeS was fitted well with the pseudo-first-order kinetic model. The negative impact of dissolved oxygen was limited, and the removal rate of Mo(VI) in the air environment is only reduced by 10% compared with the anaerobic environment. The removal rates of Mo(VI) were promoted by the presence of Ca^{2+}, Mg^{2+}, Zn^{2+}, and K^{+}, and were almost unaffected by HCO_3^-, SO_4^{2-}, and NO_3^-, while greatly inhibited by the presence of PO_4^{3-}. The increase of temperature favored Mo(VI) immobilization, suggesting the process of Mo(VI) removal was an endothermic process. This study showed that FeS could be used as an environmentally friendly agent for Mo(VI) removal in contaminated water.

Keywords: Iron sulfide; Hexavalent molybdenum; Kinetics; Influence factors; Reduction

1. Introduction

Molybdenum (Mo) is not only an indispensable trace element for humans, animals and plants but also being widely used in industrial production. With the fast development of industry, Mo pollution of surface waters has become an urgent environmental problem and caused serious molybdenum pollution in some areas, such as San Joaquin Valley, USA; Brenda Mines, Canada; and Wujintang Reservoir, China [1]. Mo(II–VI) are the main oxidation states of Mo in water solution, while molybdate ion (MoO_4^{2-}) is much more toxic and mobile that would cause growth retardation, hypothyroidism, and liver and kidney abnormalities [2,3]. The maximum contaminant level for Mo(VI) in the drinking water reached 0.07 mg/L according to the People's Republic of China (PRC), so seeking a suitable method for Mo(VI) removal from aqueous solutions has become a growing concern for sustainable use of molybdenum resources.

Currently, many methods, for example, adsorption [4], chemical precipitation [5], and ion-exchange [6], have been developed for Mo ions pollution control in aqueous solutions. Among these methods, adsorption has gained wide acceptance because of its high efficiency and low cost [7]. However, it is worth noting that the removal of molybdenum

* Corresponding author.

by adsorption possibly resulting in the release of Mo to the environment [8,9]. Moreover, the removal of Mo(VI) in water is mainly focused on the aerobic environments at present, and there is insufficient research on its removal in anaerobic environments such as groundwater, as well as the bottom layers of rivers and lakes. Reduction of Mo(VI) to form solid phases with low solubility is a more reliable and thorough removal method [10]. Therefore, developing a low-cost and environmentally-friendly reductant with higher Mo(VI) removal capacity in anaerobic water is of importance and urgency.

In recent years, chalcogenides, as a strong reducing agent, have been focused on the removal of heavy metals in wastewater, such as the removal of Cr(VI) by CdS [11], $Snln_4S_8$ nanoparticles [12], and other intercalation chalcogenides [13–15]. Iron sulfide (FeS) minerals are important natural reductants and widely present in hypoxic environments such as soil, river sediments, groundwater and offshore. Meanwhile, pyrite in the sediments mainly include amorphous FeS, tetragonal pyrite $Fe_{0.995\sim1.023}S$, Fe_3S_4, and FeS_2. Among them, amorphous FeS has a stronger reducing ability, and it has been widely applied for the treatment of heavy metals, including As(III) [16], Hg(II) [17,18], Cd(II), Co(II), Ni(II) [19] under anaerobic environment due to its unique surface chemical properties and molecular structure [20]. Typically, the metals are removed through sorption, ion exchange, and/or precipitation of highly insoluble metal sulfides [21]. FeS is an important reductant providing a source of Fe(II) and S(-II) species, which can act as electron donors and is favorable to Cr(VI) removal [22]. Therefore, FeS may facilitate Mo(VI) removal in theory. However, until now, there were few studies on the removal of Mo(VI) by FeS. Moreover, the factors such as pH, dissolved oxygen (DO), co-existing ions, and temperature govern the Mo(VI) removal rate are still unclear, which have a significant effect on the reaction.

The overall goal of this work was to investigate the feasibility of using FeS for Mo(VI) removal from aqueous solution. Characterization techniques including transmission electron microscopy with an energy-dispersive X-ray (TEM-EDS), and X-ray photoelectron spectrometer (XPS) were conducted to characterize the material composition and elucidate mechanisms governing the removal process. Kinetics were performed to discuss the removal property on FeS. The influence of experimental conditions such as FeS dosage, Mo(VI) concentration, pH, DO, co-existing ions, and temperature were investigated to explore the effectiveness of Mo(VI) removal. This study could facilitate the development of a remedial option that can be employed in anoxic Mo-contamination environments.

2. Materials and methods

2.1. Synthesis and characterization of FeS

Chemicals used in this study were of analytical grade (S1 in Supplementary information). FeS was synthesized by mixing $FeCl_2$ and Na_2S under N_2 (99.99%) protection in a three-necked flask, according to the method described in Li et al. [23] with minor adjustments. In brief, 250 mL of 0.2 M Na_2S was slowly added into 250 mL of 0.2 M $FeCl_2$ in a container on a magnetic stir plate. After aging for 3 d, the black nanoparticles were collected and washed with nanopure water three times. The freshly prepared FeS was stored in ethanol at 277 K to prevent the materials from oxidization. The particles were dried in a vacuum oven for 1 d prior to their use and characterizations.

2.2. Batch experiments of Mo(VI) removal

Batch experiments were conducted to quantify the transformation rate for Mo(VI) in the presence of FeS under different influence factors. A series of FeS suspensions were reacted with Mo(VI) (5–50 mg/L Mo) as a function of suspension density (20–200 mg/L) at an optimum pH. In addition, the Mo(VI) solutions were purged with nitrogen gas for 30 min before the addition of FeS to exclude oxygen. The ionic strength of the Mo(VI) solution was adjusted by 0.1 mol/L NaCl to an invariable value. To simulate oxygen-limited conditions, batch experiments were conducted in 100 mL headspace vials with Teflon-lined caps wrapped with aluminum foil. To investigate the effect of DO, the nitrogen and pure oxygen conditions were achieved by exposing nitrogen and pure oxygen to Mo(VI) solutions for 30 min prior to the addition of FeS, respectively. Uninterrupted shaking was carried out during the experiments with a constant speed of 180 rpm, and the blank samples performed the same procedure. At certain time intervals of this reaction, 2.0 mL of solution sample was periodically withdrawn from each reactor with a glass syringe and then filtered through a 0.45 μm membrane for immediate analysis. All the tests were repeated three times, and the average values were presented in tables and figures.

To evaluate the Mo(VI) removal efficiency, the data were analyzed by simulating the pseudo-first-order reaction model, pseudo-first and second-order adsorption models [24,25], which were provided in Supporting Information (S2). To test the influence of the initial pH on removal behavior, the initial pH of the Mo(VI) solutions was adjusted by using 1 mol/L H_2SO_4 or 1 mol/L NaOH additions, and the total volume that had been changed was <2%. The influences of co-existing ions (PO_4^{3-}, HCO_3^-, SO_4^{2-}, NO_3^-, Ca^{2+}, Mg^{2+}, Zn^{2+}, K^+; used as their respective 0.1 mmol/L sodium salts or chlorate) and temperature (283, 293, 303, and 313 K) on the removal efficiency of Mo(VI) by FeS were also investigated, and these experiments were conducted under similar experimental conditions as described above. The experiment conditions used to study the effects of co-existing ions and temperature were kept constant: Mo(VI) concentration, FeS dosage and pH were kept at 10 mg/L, 100 mg/L, and 4, respectively.

2.3. Analytical methods

Separate experiments were conducted to study the changes in the surface morphology and structure of FeS before and after reaction with Mo(VI). After the reaction reached equilibrium, the FeS suspensions were centrifuged at 10,000 rpm for 10 min and the FeS solids were dried under N_2, and used for surface analysis. The details of analytical methods are shown in S3 in Supplementary Information.

3. Results and discussion

3.1. Mo(VI) removal kinetics

As shown in Fig. 1, the initial concentrations of FeS and Mo(VI) significantly influenced the removal of Mo(VI), and a significant increase of Mo(VI) removal efficiency from 21.85% to 76.41% with a decrease of Mo(VI) initial concentration from 50 to 5 mg/L within 240 min of reaction. Since the available adsorption sites on FeS were fixed, more adsorption sites were required for the complete removal with the increase of Mo(VI) concentration. Besides, the removal efficiency of Mo(VI) increased rapidly from 13.95% to 84.20% within 240 min of reaction as FeS dosage increased from 20 to 200 mg/L (Fig. 1c). This phenomenon can be explained by the increased surface area and reaction sites on FeS particles, the removal of Mo(VI) was thus accelerated [26].

With reference to existing studies, it is known that the removal of Mo(VI) by Fe-based materials is a multi-step process, including electrostatic adsorption and subsequent Mo(VI) reduction [27,28]. Therefore, pseudo-first and second-order models were used to fit the reaction. As shown in Figs. 1b and d, the experimental data agree well with the pseudo-first-order reaction kinetic model. Linear regression analysis was used to determine the kinetic parameters, and the results are shown in Table 1. According to the simulated correlation coefficient, the pseudo-first-order and second-order adsorption models do not seem to be suitable for describing the removal of Mo(VI), while the pseudo-first-order kinetic models perform better with high correlation coefficients ($R^2 > 0.90$). Besides, with the increase of FeS, the reaction rate constant (k_{obs}) gradually increases, and the value of k_{obs} at 200 mg/L of FeS dosage was 26 times than of 20 mg/L FeS (Fig. 1d). While the values of k_{obs} gradually decreased as MoO_4^{2-} initial concentration increased (Fig. 1b). The results indicated that reduction was probably the rate-limiting step for Mo(VI) removal because the reduction of contaminants follows the pseudo-first-order kinetic model [23].

3.2. Surface analysis of FeS

To further elucidate the surface reaction mechanisms of FeS with Mo(VI), surface analysis of FeS was performed. The morphology and structure of FeS before and after Mo(VI) treatment were characterized by TEM (Fig. 2). Obviously, there were abundant irregular shapes of micropores among FeS layer before Mo(VI) treatment (B-FeS),

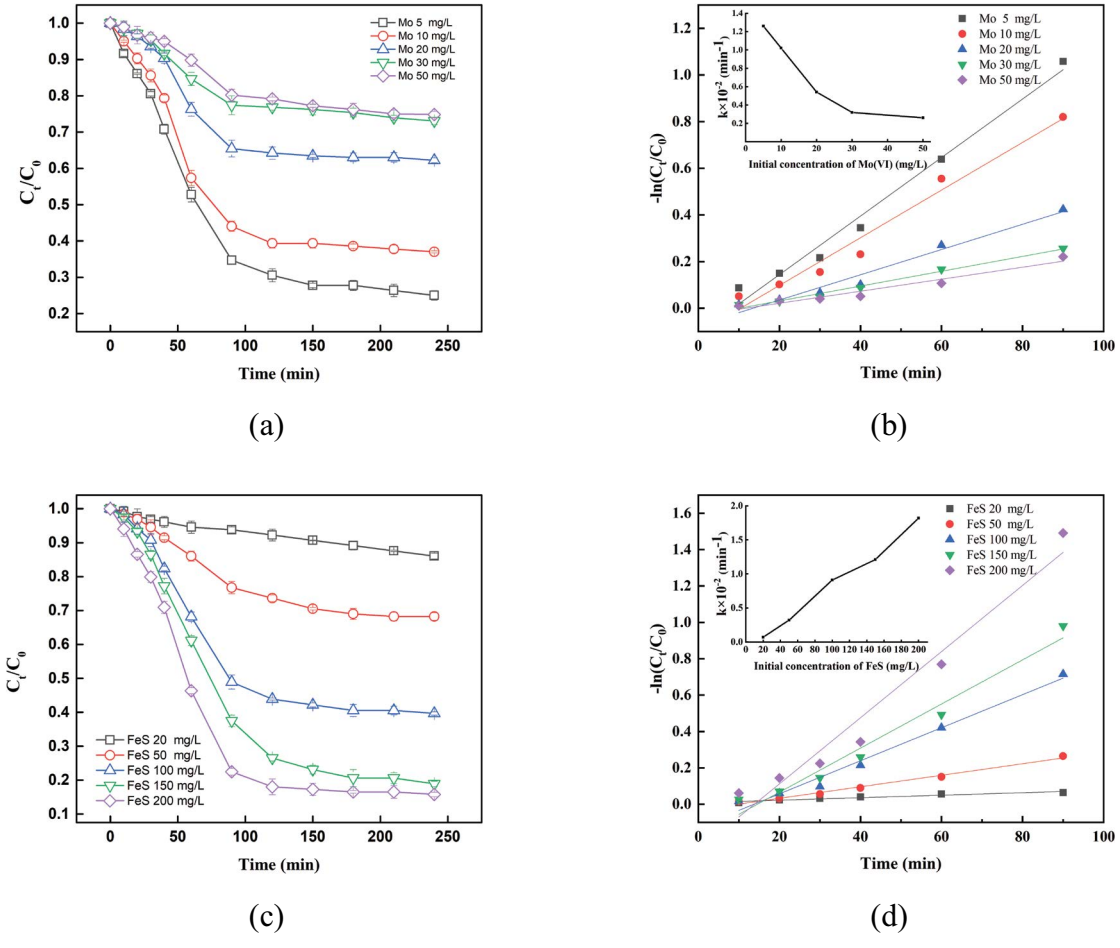

Fig. 1. (a,b) Effect of initial Mo(VI) concentration, and (c,d) FeS dosage on Mo(VI) removal rate (T = 298 K; (a,b) 100 mg/L FeS; (c,d) 10 mg/L Mo(VI); pH = 4).

Table 1
Comparison of the pseudo-first and second-order kinetics constants for Mo(VI) removal by FeS particles (T = 298 K, initial pH = 4)

Parameter		Initial concentration of Mo(VI) (mg/L)					Initial concentration of FeS (mg/L)				
		5	10	20	30	50	20	50	100	150	200
Pseudo-first-order reaction kinetics	$k_{obs} \times 10^{-2}$ (min^{-1})	1.26	1.02	0.54	0.32	0.26	0.07	0.32	0.91	1.21	1.82
	R^2	0.979	0.966	0.962	0.983	0.936	0.911	0.985	0.978	0.964	0.952
Pseudo-first-order adsorption kinetics	$k_1 \times 10^{-2}$ (min^{-1})	1.06	1.18	1.33	0.98	0.79	0.29	0.69	1.02	0.79	1.33
	q_e (mg/g)	103.73	96.86	68.41	39.10	34.48	13.38	40.16	90.98	108.94	142.43
	R^2	0.940	0.933	0.885	0.931	0.846	0.946	0.932	0.932	0.937	0.896
Pseudo-second-order adsorption kinetics	$k_2 \times 10^{-2}$ (g/mg/min)	0.01	0.75	4.81	4.38	4.96	4.19	3.51	4.37	2.80	0.67
	q_e (mg/g)	9615.39	132.63	20.79	22.83	20.15	23.90	28.47	22.88	35.69	150.38
	R^2	0.0006	0.629	0.871	0.799	0.639	0.745	0.838	0.537	0.633	0.783

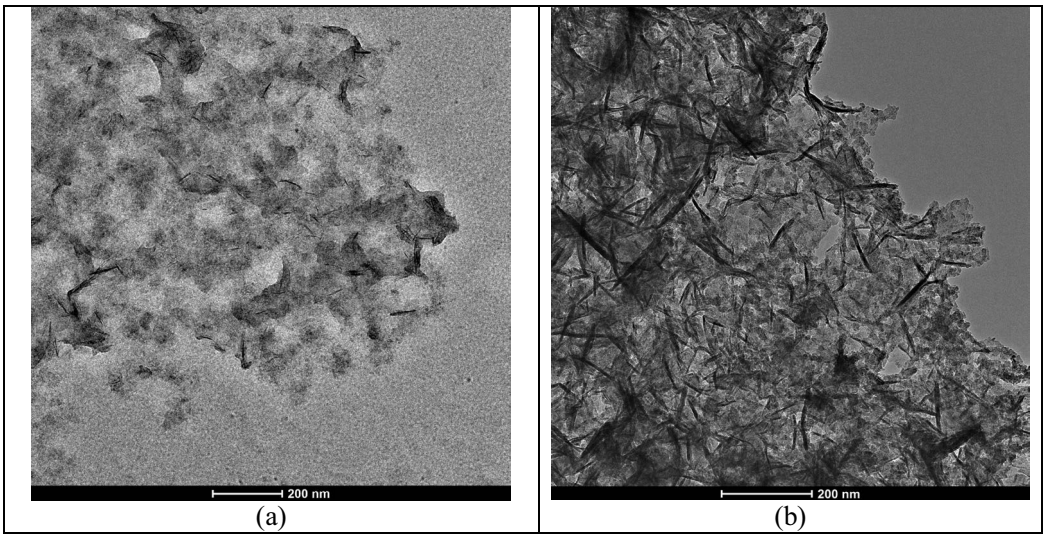

Fig. 2. Transmission electron microscopy images of FeS before (a) and after Mo(VI) treated FeS (b) (T = 298 K; 10 mg/L Mo(VI); 100 mg/L FeS; pH = 4).

which was consistent with poorly crystalline mackinawite (Fig. 2a) [29]. While the denser structure was formed on the surface of FeS after reacted with Mo(VI) (Mo-FeS) (Fig. 2b), indicating that the imbedding of molybdenum changed FeS surface morphology to some extent. EDS analysis was conducted to show the element type and content composition of FeS before and reacted with Mo(VI) at pH 4 (Table S1). The atomic fraction of Fe and S in B-FeS was around 1:1. However, the atomic fraction of Fe and S in Mo-FeS was declined, while Mo atomic fraction in Mo-FeS was increased, which indicated that part of Mo was immobilization successfully on FeS. The mapping images show the distribution of the element on the sample, and more dots indicate more of the element. As shown in Fig. S1, mapping images of Mo-FeS matched the results of EDS, which also indicated that Mo was evenly distributed inside the FeS. Furthermore, the FeS size (117.13 nm) was decreased significantly under acidic conditions (pH 4) compared with the original FeS (579.43 nm), which is more conducive to the reaction with Mo(VI) at pH 4.

X-ray diffraction analysis indicated that the fresh synthetic FeS solid might be poorly crystalline mackinawite (Fig. 3), being consistent with the finding of Li et al. [23]. However, the oxidized FeS had the typical diffraction peaks for lepidocrocite, which suggested the occurrence of mineral interactions between FeS and Fe oxide coatings. Previous studies also verified that the formation of more crystalline lepidocrocite was suspected to be induced by the electron transfer between FeS and Fe oxide coatings [30]. XPS analysis was performed to obtain Mo species of particle surface. The typical peak of Mo3d on the surface of FeS was observed after Mo(VI) treatment (Fig. 4a), which indicated the incorporation of Mo into the particles. The Mo 3d spectrum was dominated by a doublet with a Mo $3d_{5/2}$ binding energy of 229.82 eV and 230.80–232.85 eV, which was attributed to the Mo^{IV} ion in MoS_2 [31], and Mo^{V} [32], respectively (Fig. 4b). A similar phenomenon was reported by Chen et al. who employed XPS to investigate the interaction of sulfate-reducing bacteria with Mo, and they find the Mo3d spectrum from the culture droplets showed that a dominant amount of Mo existed as Mo^{5+} [33]. Obviously, removed Mo(VI) is mainly removed by reduction of FeS at pH 4, which was consistent with the result of the kinetics model.

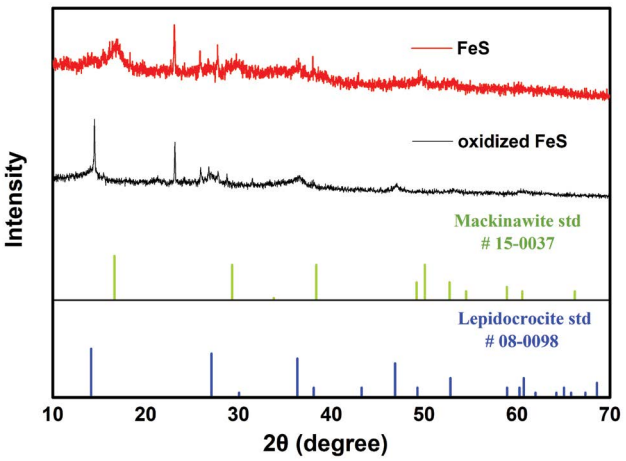

Fig. 3. X-ray diffraction pattern of the synthetic FeS and oxidized FeS.

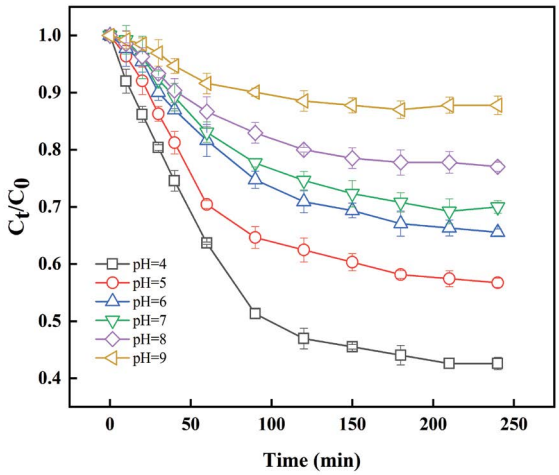

Fig. 5. Effect of the initial pH on Mo(VI) removal by FeS particles (T = 298 K; 10 mg/L Mo(VI); 100 mg/L FeS).

3.3. *Effect of pH*

The pH of the solution is an important control variable for Mo(VI) adsorption and reduction. Fig. 5 shows the Mo(VI) absorption performance of FeS particles at different initial pH values, ranging from 4 to 9. In general, the removal rate of Mo(VI) increases with decreasing pH, which is similar to the removal rate previously described in different Fe systems [3,10,27]. The pH effect was revealed by monitoring the pH changes before and after the reaction (Fig. S2). Regardless of the initial pH value, except for pH 9, in most cases, the pH value of the solution increases during the reaction, and the final pH value is between 6.15 and 7.14. For example, when the initial pH was 4, the pH increased to 6.15 after 240 min of reaction. The phenomenon of increasing pH indicates that hydrated hydrogen ion (H^+) is indispensable for the adsorption of Mo(VI) [34]. Mackinawite (FeS) was dissolved in the acidic environment under anoxic conditions, while the dissolution of FeS was mainly promoted by protons through Eq. (1) [35].

Besides, molybdate is also subject to pH-dependent dissolution, the predominating ionic species of Mo(VI) was $Mo_8O_{26}^{-4}$, $Mo_7O_{24}^{-6}$, and $HMo_7O_{24}^{-5}$ at pH < 7 (Fig. S3), therefore the possible reduction mechanism could be explained by Eq. (2). Moreover, this is consistent with the XPS analysis of FeS particles after the reaction with Mo(VI) when pH = 4. Under alkaline conditions, the free and surface-bound ferrous ions are more easily oxidized, forming thick hydroxide layers on the surface [36]. In addition, FeS particles would be negatively charged in an alkaline solution, hindering the Mo(VI) adsorption due to electrostatic repulsion. The alkaline conditions would be conductive to the adsorptive removal of Mo species due to the co-precipitation of Fe(III)/Mo hydroxide via Eq. (3) [10].

$$FeS(s) + 2H^+ = Fe^{2+} + H_2S(aq) \quad (1)$$

$$Fe^{2+} + Mo_7O_{24}^{-6}/Mo_8O_{26}^{-4}/HMo_7O_{24}^{-5} + HS^- + H^+ \rightarrow Fe^{3+} + MoS_2 + Mo^{V}O_xS_y + H_2O \quad (2)$$

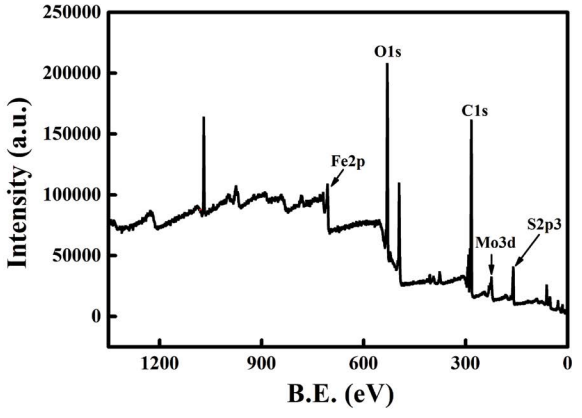

(a)

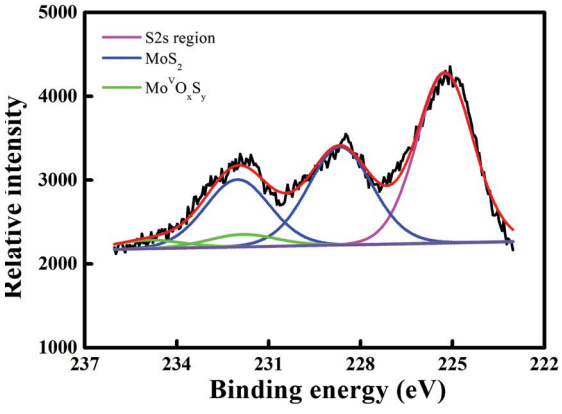

(b)

Fig. 4. (a) X-ray photoelectron spectrometer of the surfaces of Mo(VI) treated FeS, (b) narrow scan of Mo3d of Mo(VI) treated FeS (T = 298 K; 10 mg/L Mo(VI); 100 mg/L FeS; pH = 4).

$$\equiv Fe\text{-}OH + MoO_4^{2-} = \equiv Fe\text{-}O_2MoO_2^- + OH^- \quad (3)$$

3.4. Effect of dissolved oxygen

DO is typically present in surface water and shallow groundwater. To investigate the impact of DO on Mo(VI) removal by FeS, experiments were conducted and the results are shown in Fig. 6. The presence of oxygen significantly depressed Mo(VI) removal, and Mo(VI) removal rate from high to low was nitrogen > air > pure oxygen. Oxygen would compete directly with Mo(VI) to consume surface Fe(II) species at acid solution as explained in Eq. (4), which was confirmed in Fig. 6. The ratio of Fe^{3+} in total dissolve Fe ions increased in nitrogen condition because of Mo(VI) reduction, while it was contrary in air and pure oxygen condition for the co-precipitation or adsorption of Mo(VI) removal [3]. The reactivity of FeS decreased after reacting with dissolved oxygen. However, this negative impact was limited because 70% Mo(VI) was still removed after 4 h of reaction by the FeS particles in air condition, which may be due to the adsorption of Mo(VI) by divalent and trivalent iron [3].

$$4Fe^{2+} + O_2 + 4H^+ = 4Fe^{3+} + 2H_2O \quad (4)$$

3.5. Effect of co-existing ions

The co-existing ions typically exist in groundwater and industrial wastewater may potentially compete with the reaction. In this study, the effect of eight common ions in natural water bodies on Mo(VI) removal efficiency was investigated (Fig. 7). All the co-existing cations promoted the Mo(VI) removal by FeS, being consistent with the finding of Lv et al. [37], and the removal efficiencies were all above 75% after a 4 h reaction. This was due to the fact the FeS was positively charged during the reaction process at pH 4, and offered electrostatic repulsion to the positively charged cations, thus inhibiting their competition with Mo(VI) for the active site on FeS. Furthermore, the standard reduction potential of Ca^{2+}, Mg^{2+}, Zn^{2+}, and K^+ (E_0 = –2.76 V, –2.37 V, –0.76 V and –2.92 V, respectively) is lower than that of Fe^{2+} (E_0 = –0.45 V), thus the four free cations may form some covalent compound with Mo(VI). However, the specific chemical reaction process still needs further study. Except for PO_4^{3-}, the presence of anions improves the removal rate of Mo(VI). SO_4^{2-} and NO_3^- are considered to be low-affinity ligands, forming an outer spherical complex with iron (oxygen) hydroxide, so their competitive effects can be ignored [38]. The negative effect of HCO_3^- on Mo(VI) removal by FeS was not observed in this research, indicating that the reactivity of FeS was less susceptible to HCO_3^- [39]. However, the presence of 0.1 mM PO_4^{3-} reduced the Mo(VI) removal efficiency by about 30%. PO_4^{3-} had a similar structure and size as $HMo_7O_{24}^{-5}$, thus the competition between PO_4^{3-} and Mo(VI) for active sites on the FeS affected the Mo(VI) removal [36]. In addition, PO_4^{3-} forms an inner-sphere complex with iron (oxygen) hydroxide, reducing the removal ability of Mo(VI) [9]. Therefore, the presence of PO_4^{3-} obviously hinders the removal of Mo(VI).

3.6. Effect of reaction temperature

The removal of Mo(VI) by FeS was also dependent on the reaction temperature. As shown in Fig. 8a, the removal rate of Mo(VI) promoted from 35.48% to 62.63% with the increase of temperature (from 283 K to 313 K), indicating the Mo(VI) removal process to be endothermic. This may be due to the fact that temperature rise may accelerate Mo(VI) reduction by overcoming high activation barriers. A similar trend had been reported for the removal of Mo(VI) [7,34]. However, Mo(VI) removal rate remained almost unchanged when the reaction temperature increased from 303 K to 313 K, which mainly due to FeS was more easily oxidized at a higher temperature, thereby reducing the active sites that react with Mo(VI). Besides, the correlation coefficients (R^2) confirm the fit of experimental data by the pseudo-first-order reaction model (Fig. 8b).

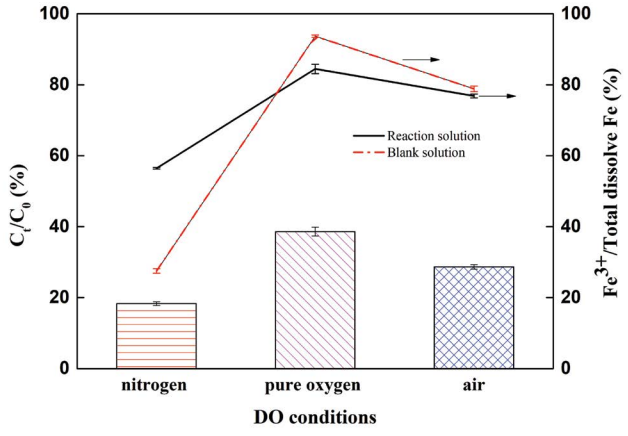

Fig. 6. Comparison of Mo(VI) removal by FeS particles under different dissolve oxygen conditions (10 mg/L Mo(VI); 200 mg/L FeS; pH = 4.0; reaction solution referred to the FeS solution after reaction with Mo(VI); blank solution referred to FeS solution without Mo(VI); T = 298 K).

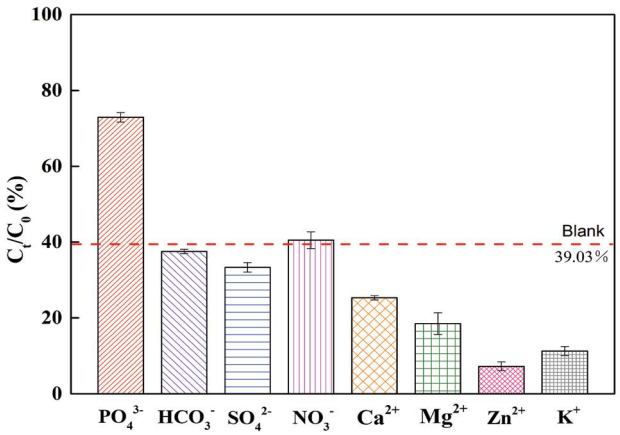

Fig. 7. Effect of co-existing ions on Mo(VI) removal by FeS (T = 298 K; 10 mg/L Mo(VI); 100 mg/L FeS; pH = 4; 0.1 mM ion concentration; blank referred to FeS reaction solution without the above co-existing ions).

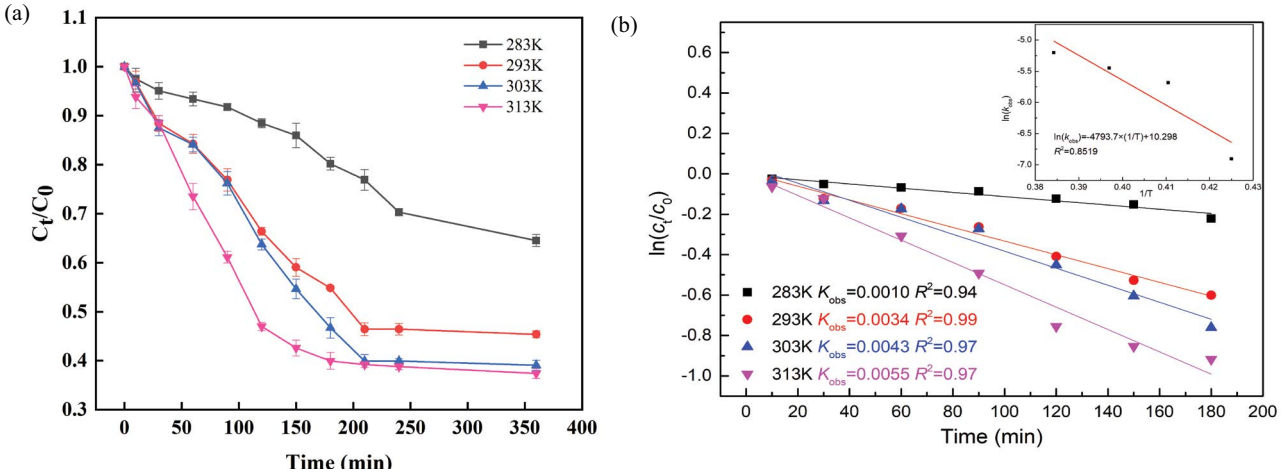

Fig. 8. (a) Effect of temperature on Mo(VI) removal by FeS; (b) pseudo-first-order reaction model fit for Mo(VI) immobilization onto FeS at various temperature, inset: Arrhenius plot of ln(k_{obs}) to 1/T (10 mg/L Mo(VI); 100 mg/L FeS; pH = 4).

Moreover, the apparent rate constant (k_{obs}) gradually declines along with the falling of temperature. The apparent activation energy (E_a) is usually used to distinguish between physical adsorption and chemical reaction, and the value of physical adsorption is usually less than 4.2 kJ/mol [40]. The value of E_a calculated by the Arrhenius equation (Eq. 5) was 39.86 kJ/mol, which indicates that Mo(VI) removal by FeS is through a chemical reaction. This is also consistent with the above research results that Mo(VI) removal is mainly achieved by chemical reduction.

$$\ln k_{obs} = \frac{-E_a}{RT} + \ln A \quad (5)$$

where k_{obs} (min^{-1}) and E_a (kJ/mol) are defined as apparent rate constant and apparent activation energy; R (8.314 J/(mol K)) is molar gas constant; T (K) represents temperature and A (min^{-1}) is pre-exponential factor.

4. Conclusions

The prepared FeS was rapid and competent for Mo(VI) removal from solutions. The systematic investigation was carried on for the Mo(VI) removal under various conditions. The removal kinetic process of Mo(VI) abided by the pseudo-first-order kinetic model within 4 h. XPS analysis demonstrated that the Mo(VI) was immobilized through reduction at pH 4, as evidenced by no Mo(VI) existence. The increasing solution pH from 4 to 9 significantly decreased Mo(VI) removal by FeS. The presence of DO had limited effect on Mo(VI) removal, and 70% Mo(VI) was still removed by FeS particles in air condition. The competitive influence of co-existing ions was negligible except PO_4^{3-}, which reduced Mo(VI) removal efficiency by about 30%. The Mo(VI) removal process was endothermic, and the activation energy value indicates that Mo(VI) was chemically immobilized on FeS. The findings in this study indicate that FeS nanoparticles hold the promise to be employed as an effective reductant for immobilization of Mo(VI) in anaerobic environment.

Acknowledgements

This work was financially supported by the National Natural Science Foundation of China (No. 51709001), Key R&D Program of Ningxia Hui Autonomous Region (Special Project for S&T Cooperation with unit outside the province in 2019) (2019BFG02028), and the Provincial and National College Student Innovation and Entrepreneurship Training Program of Anhui University of Technology (No. S201910360324, 202010360091).

References

[1] J.J. Lian, S.G. Xu, N.-B. Chang, C.W. Han, J.W. Liu, Removal of molybdenum(VI) from mine tailing effluents with the aid of loessial soil and slag waste, Environ. Eng. Sci., 30 (2013) 213–220.
[2] C. Namasivayam, D. Sangeetha, Removal of molybdate from water by adsorption onto $ZnCl_2$ activated coir pith carbon, Bioresour. Technol., 97 (2006) 1194–1200.
[3] J.J. Lian, F.J. Zhou, B. Chen, M. Yang, S.S. Wang, Z.L. Liu, S.P. Niu, Enhanced adsorption of molybdenum(VI) onto drinking water treatment residues modified by thermal treatment and acid activation, J. Cleaner Prod., 244 (2020) 118719, https://doi.org/10.1016/j.jclepro.2019.118719.
[4] W.J. Shan, Y.N. Shu, H. Chen, D.Y. Zhang, W. Wang, H.Q. Ru, Y. Xiong, The recovery of molybdenum(VI) from rhenium(VII) on amino-functionalized mesoporous materials, Hydrometallurgy, 165 (2016) 251–260.
[5] R. Mamtaz, D.H. Bache, Reduction of arsenic in groundwater by coprecipitation with iron, J. Water Supply Res. Technol. AQUA, 50 (2001) 313–324.
[6] I. Polowczyl, P. Cyganowski, B.F. Urbano, B.L. Rivas, M. Bryjak, N. Kabay, Amberlite IRA-400 and IRA-743 chelating resins for the sorption and recovery of molybdenum(VI) and vanadium(V): equilibrium and kinetic studies, Hydrometallurgy, 169 (2017) 496–507.
[7] Z.N. Lou, J. Wang, X.D. Jin, L. Wan, Y. Wang, H. Chen, W.J. Shan, Y. Xiong, Brown algae based new sorption material for fractional recovery of molybdenum and rhenium from wastewater, Chem. Eng. J., 273 (2015) 231–239.
[8] F.A. Bertoni, A.C. Medeot, J.C. Gonzalez, L.F. Sala, S.E. Bellu, Application of green seaweed biomass for Mo(VI) sorption from contaminated waters. Kinetic, thermodynamic and continuous sorption studies, J. Colloid Interface Sci., 446 (2015) 122–132.

[9] N. Xu, C. Christodoulatos, W. Braida, Adsorption of molybdate and tetrathiomolybdate onto pyrite and goethite: effect of pH and competitive anions, Chemosphere, 62 (2006) 1726–1735.
[10] B.C. Bostick, S. Fendorf, Differential adsorption of molybdate and tetrathiomolybdate on pyrite (FeS_2), Environ. Sci. Technol., 37 (2003) 285–291.
[11] R.C. Pawar, C.S. Lee, Sensitization of CdS nanoparticles onto reduced graphene oxide (RGO) fabricated by chemical bath deposition method for effective removal of Cr(VI), Mater. Chem. Phys., 141 (2013) 686–693.
[12] P.F. Xu, S.Y. Huang, Y.C. Lv, Y. Chen, M.H. Liu, H.J. Fan, Surfactant-assisted hydrothermal synthesis of rGO/$SnIn_4S_8$ nanosheets and their application in complete removal of Cr(VI), RSC Adv., 8 (2018) 5749–5759.
[13] K. Gupta, B.L. Yuan, C. Chen, N. Varnakavi, M.L. Fu, $K_{2x}Mn_xSn_{3-x}S_6$ (x = 0.5–0.95) (KMS-1) immobilized on the reduced graphene oxide as KMS-1/r-GO aerogel to effectively remove Cs^+ and Sr^{2+} from aqueous solution, Chem. Eng. J., 369 (2019) 803–812.
[14] J.R. Li, X. Wang, B.L. Yuan, M.L. Fu, H.J. Cui, Robust removal of heavy metals from water by intercalation chalcogenide $[CH_3NH_3]_{2x}Mn_xSn_{3-x}S6{\cdot}0.5H_2O$, Appl. Surf. Sci., 320 (2014) 112–119.
[15] J.R. Li, X. Wang, B.L. Yuan, M.L. Fu, Layered chalcogenide for Cu^{2+} removal by ion-exchange from wastewater, J. Mol. Liq., 200 (2014) 205–212.
[16] Y.S. Han, H.J. Seong, C.M. Chon, J.H. Park, I.H. Nam, K. Yoo, J.S. Ahn, Interaction of Sb(III) with iron sulfide under anoxic conditions: similarities and differences compared to As(III) interactions, Chemosphere, 195 (2018) 762–770.
[17] Y. Gong, Y. Liu, Z. Xiong, D. Zhao, Immobilization of mercury by carboxymethyl cellulose stabilized iron sulfide nanoparticles: reaction mechanisms and effects of stabilizer and water chemistry, Environ. Sci. Technol., 48 (2014) 3986–3994.
[18] M.X. Wang, Y.L. Li, D.Y. Zhao, L. Zhuang, G.Q. Yang, Y.Y. Gong, Immobilization of mercury by iron sulfide nanoparticles alters mercury speciation and microbial methylation in contaminated groundwater, Chem. Eng. J., 381 (2020) 122664, https://doi.org/10.1016/j.cej.2019.122664.
[19] A. Afkhami, T. Madrakian, A. Amini, Mo(VI) and w(VI) removal from water samples by acid-treated high area carbon cloth, Desalination, 243(2009) 258–264.
[20] M.J. Wharton, B. Atkins, J.M. Charnock, F.R. Livens, R.A.D. Pattrick, D. Collison, An X-ray absorption spectroscopy study of the coprecipitation of Tc and Re with mackinawite (FeS), Appl. Geochem., 15 (2000) 347–354.
[21] Y. Gong, J. Tang, D. Zhao, Application of iron sulfide particles for groundwater and soil remediation: a review, Water Res., 89 (2016) 309–320.
[22] F. Demoisson, M. Mullet, B. Humbert, Pyrite oxidation by hexavalent chromium: investigation of the chemical processes by monitoring of aqueous metal species, Environ. Sci. Technol., 39 (2005) 8747–8752.
[23] D. Li, P.A. Peng, Z.Q. Yu, W.L. Huang, Y. Zhong, Reductive transformation of hexabromocyclododecane (HBCD) by FeS, Water Res., 101 (2016) 195–202.
[24] P. Ganesan, R. Kamaraj, S. Vasudevan, Application of isotherm, kinetic and thermodynamic models for the adsorption of nitrate ions on graphene from aqueous solution, J. Taiwan Inst. Chem. Eng., 44 (2013) 808–814.
[25] R. Kamaraj, P. Ganesan, S. Vasudevan, Removal of lead from aqueous solutions by electrocoagulation: isotherm, kinetics and thermodynamic studies, Int. J. Environ. Sci. Technol., 12 (2015) 683–692.
[26] Y.Y. Gong, L.S. Gai, J.C. Tang, J. Fu, Q.L. Wang, E.Y. Zeng, Reduction of Cr(VI) in simulated groundwater by FeS-coated iron magnetic nanoparticles, Sci. Total Environ., 595 (2017) 743–751.
[27] D.X. Qian, Y.M. Su, Y.X. Huang, H.Q. Chu, X.F. Zhou, Y.L. Zhang, Simultaneous molybdate (Mo(VI)) recovery and hazardous ions immobilization via nanoscale zerovalent iron, J. Hazard. Mater., 344 (2018) 698–706.
[28] Y.H. Huang, C.L. Tang, H. Zeng, Removing molybdate from water using a hybridized zero-valent iron/magnetite/Fe(II) treatment system, Chem. Eng. J., 200–202 (2012) 257–263.
[29] X.L. An, F.G. Huang, H.T. Rend, Y.F. Wang, Y. Chen, Z.M. Liu, H.W. Zhang, X. Han, Oxidative dissolution of amorphous FeS and speciation of secondary Fe minerals: effects of pH and As(III) concentration, Chem. Geol., 462 (2017) 44–54.
[30] D.D. Boland, R.N. Collins, C.J. Miller, C.J. Glover, T.D. Waite, Effect of solution and solid-phase conditions on the Fe(II)-accelerated transformation of ferrihydrite to lepidocrocite and goethite, Environ. Sci. Technol., 48 (2014) 5477–5485.
[31] H. Vrubel, X. Hu, Growth and activation of an amorphous molybdenum sulfide hydrogen evolving catalyst, ACS Catal., 3 (2013) 2002–2011.
[32] P. Delporte, F. Meunier, C. Pham-Huu, P. Vennegues, M.J. Ledoux, J. Guille, Physical characterization of molybdenum oxycarbide catalyst: TEM, XRD and XPS, Catal. Today, 23 (1995) 251–267.
[33] G. Chen, T.E. Ford, C.R. Clayton, Interaction of sulfate-reducing bacteria with molybdenum dissolved from sputter-deposited molybdenum thin films and pure molybdenum powder, J. Colloid Interface Sci., 204 (1998) 237–246.
[34] J.J. Lian, Y.G. Huang, B. Chen, S.S. Wang, P. Wang, S.P. Niu, Z.L. Liu, Removal of molybdenum(VI) from aqueous solutions using nano zero-valent iron supported on biochar enhanced by cetyl-trimethyl ammonium bromide: adsorption kinetic, isotherm and mechanism studies, Water Sci. Technol., 2017 (2018) 859–868.
[35] D. Rickard, The solubility of FeS, Geochim. Cosmochim. Acta, 70 (2006) 5779–5789.
[36] S. Zhou, Y. Li, J. Chen, Z. Liu, Z. Wang, P. Na, Enhanced Cr(VI) removal from aqueous solutions using Ni/Fe bimetallic nanoparticles: characterization, kinetics and mechanism, RSC Adv., 4 (2014) 50699–50707.
[37] D. Lv, J.S. Zhou, Z. Cao, J. Xu, Y.L. Liu, Y.Z. Li, K.L. Yang, Z.M. Lou, L.P. Lou, X.H. Xu, Mechanism and influence factors of chromium(VI) removal by sulfidemodified nanoscale zerovalent iron, Chemosphere, 224 (2019) 306–315.
[38] K.Z. Setshedi, M. Bhaumik, S. Songwane, M.S. Onyango, A. Maity, Exfoliated polypyrrole-organically modified montmorillonite clay nanocomposite as a potential adsorbent for Cr(VI) removal, Chem. Eng. J., 222 (2013) 186–197.
[39] X.M. Dou, R. Li, B. Zhao, W.Y. Liang, Arsenate removal from water by zerovalent iron/activated carbon galvanic couples, J. Hazard. Mater., 182 (2010) 108–114.
[40] A. Sari, M. Tuzen, D. Citak, M. Soylak, Equilibrium, kinetic and thermodynamic studies of adsorption of Pb(II) from aqueous solution onto Turkish kaolinite clay, J. Hazard. Mater., 149 (2007) 283–291.

Supplementary information

S1. Chemicals

Sodium sulfide ($Na_2S·9H_2O$), sodium molybdate ($Na_2MoO_4·2H_2O$), sodium nitrate ($NaNO_3$), sodium hydroxide (NaOH), and sodium chloride (NaCl) were purchased from ALADDIN Reagent Co., Ltd., (Shanghai, China). Sodium bicarbonate ($NaHCO_3$), sodium sulfate (Na_2SO_4), sodium phosphate ($Na_3PO_4·12H_2O$), potassium chloride (KCl), zinc chloride (ZnCl), calcium chloride ($CaCl_2·2H_2O$), magnesium chloride ($MgCl_2·6H_2O$) were obtained from Kermel (Tianjin, China). Molybdenum was added to suspensions using 10 mM stock solutions of $Na_2MoO_4·2H_2O$. Ferrous chloride ($FeCl_2$) was purchased from Alfa Aesar-A Johnson Matthey Company (MA, USA). The deionized water (18.2 MΩ cm) was autoclaved at 394 K for 20 min, and then purged with high purity N_2 (99.999%) for at least 30 min to remove the oxygen before used. Reagents were stored under nitrogen and used as purchased.

S2. Introduction of two kinetic models

S2.1. Pseudo-first-order reaction model

The pseudo-first-order reaction model can be expressed as Eq. (S1):

$$\ln\left(\frac{C}{C_0}\right) = -k_{obs}t \tag{S1}$$

where k_{obs} is the rate constant of pseudo-first-order kinetics (min^{-1}), C (mg/L) and C_0 (mg/L) are the concentration of Mo(VI) in aqueous solution at t min and 0 min, respectively; t is the contact time (min).

S2.2. Pseudo-first and second-order adsorption models

The pseudo-first-order adsorption model can be expressed as Eq. (S2):

$$\log\left(q_e - q_t\right) = \log\left(q_e\right) - \frac{k_1 t}{2.303} \tag{S2}$$

where k_1 is the equilibrium rate constant of pseudo-first-order kinetics (min^{-1}). The parameters q_t (mg/g) and q_e (mg/g) are the concentration of Mo(VI) adsorbed onto adsorbents at time t (min) or equilibrium time.

The linear form of the pseudo-second-order adsorption model can be expressed as Eq. (S3):

$$\frac{t}{q_t} = \frac{1}{k_2 q_e^2} + \frac{t}{q_e} \tag{S3}$$

where k_2 is the rate constant of the pseudo-second-order adsorption kinetics (g/mg/min).

S3. Analytical methods

Concentrations of Mo and total Fe ions were measured by flame atomic absorption spectrometer (ZA-3000). The concentration of Fe(II) was measured by a 1,10-phenanthroline method using a UV-vis spectrometer (Shimadzu UV-2550, Japan) at 510 nm. The morphological change and the surface elemental analysis of FeS before and after reaction with Mo(VI) at pH 4.0 was measured using a transmission electron microscopy with an energy-dispersive X-ray system at 15 kV (FEI Talos F200S). Powder X-ray diffraction patterns at two angles from 10° to 70° were recorded at an interval of 0.33° on an Ultima IV diffractometer using Cu radiation (40 kV, 40 mA). The particle sizes were measured by the Zetasizer Nano-ZS90 87 (Malvern instruments Ltd., Worcs, UK). The chemical composition and oxidation state of Mo species on the FeS surface were examined by an ESCALAB-250 X-ray photoelectron spectrometer (Thermo Electron Corp., MA, USA).

Table S1
Energy-dispersive X-ray spectroscopy analysis of FeS before and after Mo(VI) treatment at pH 4.0

Material	Atomic fraction (%)			
	O	S	Fe	Mo
B-FeS	32.27	37.14	30.56	–
Mo-FeS	51.24	23.96	22.04	2.74

B-FeS: FeS before Mo(VI) treatment; Mo-FeS: Mo(VI)-reacted FeS products; –: No data.

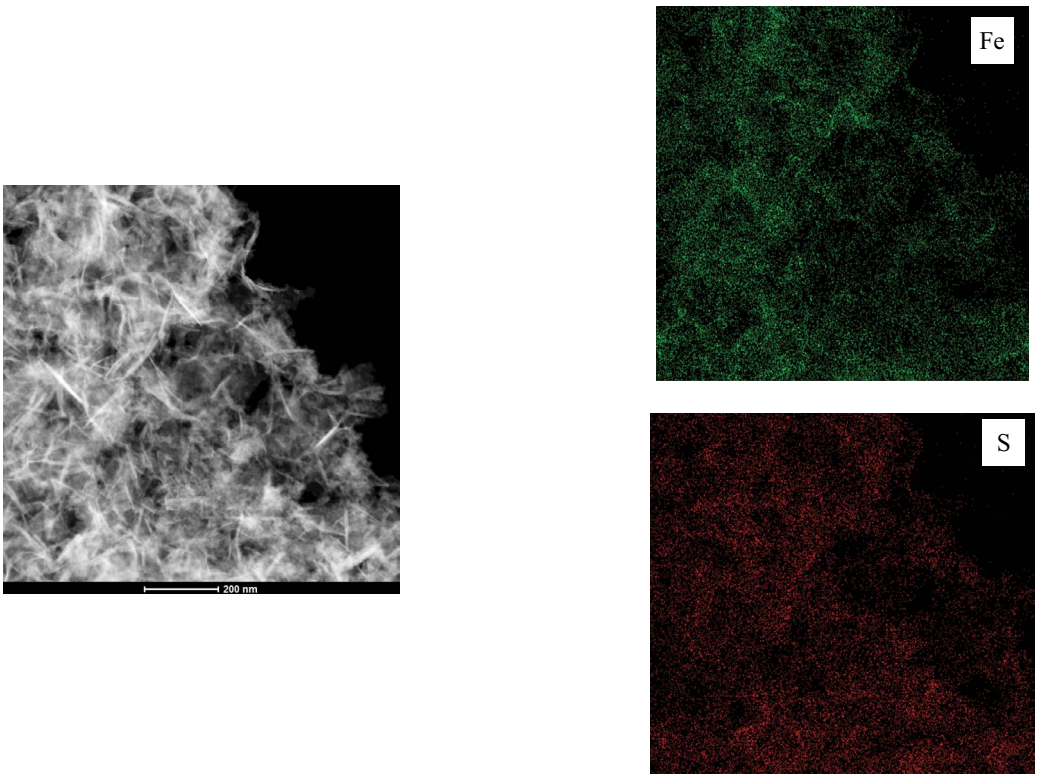

(a)

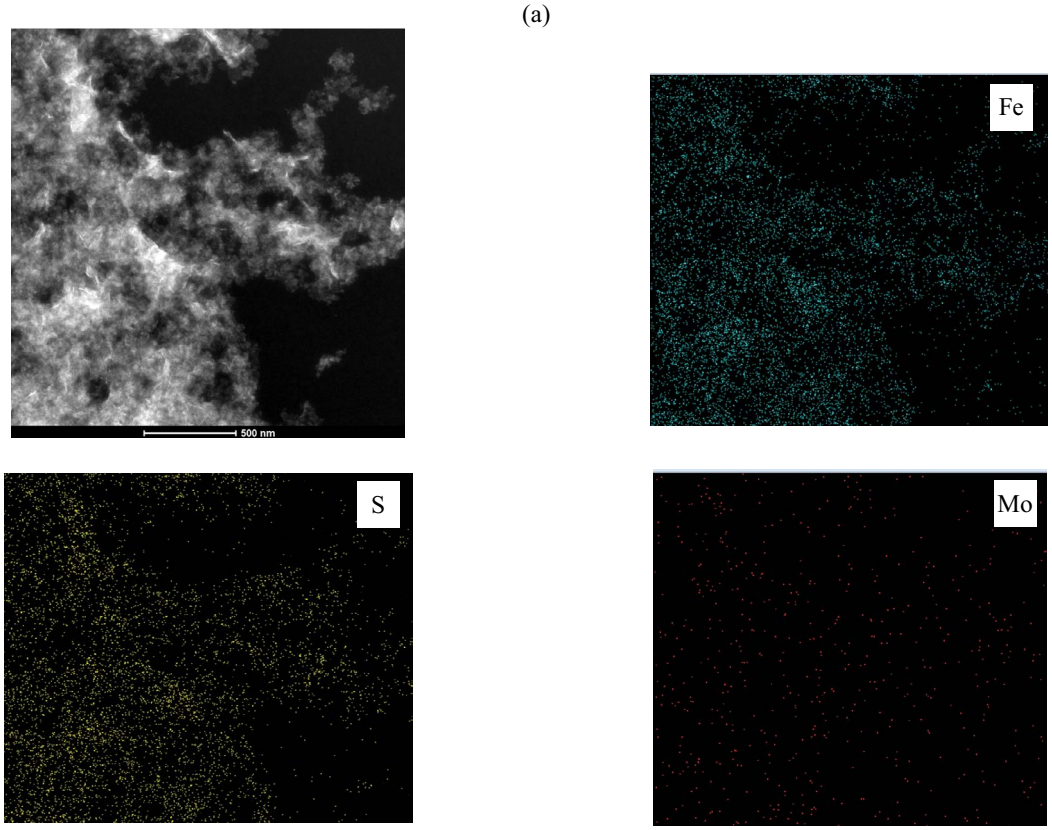

(b)

Fig. S1. Mapping images of FeS before (a) and after Mo(VI) treatment (b) at pH 4.0. Conditions: T = 298 K; 10 mg/L Mo(VI); 100 mg/L FeS.

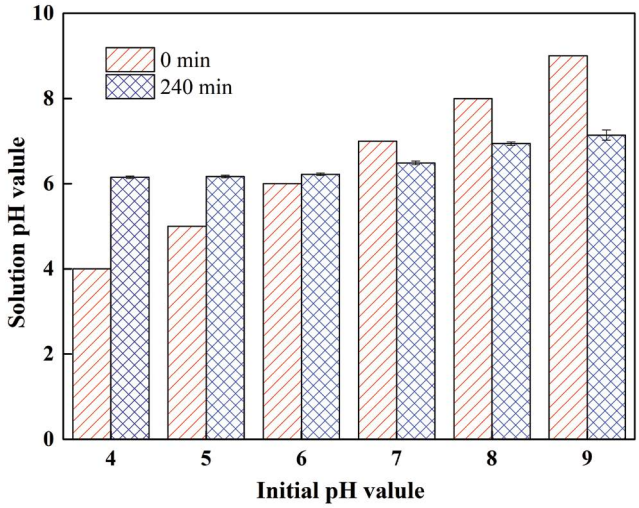

Fig. S2. Variation of solution pH during Mo(VI) reduction with different initial pH values.

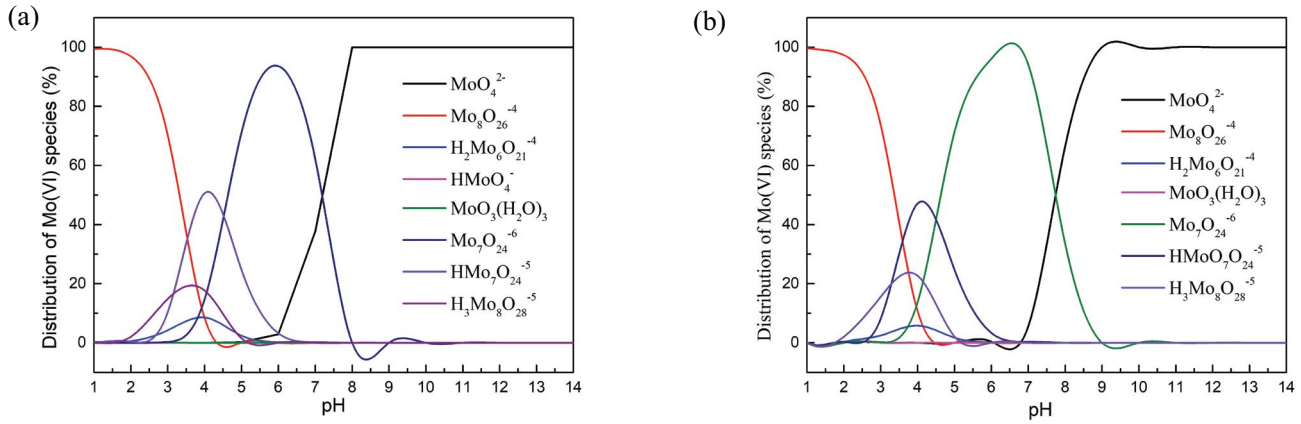

Fig. S3. Distribution of molybdate species as a function of pH at Mo(VI) concentration of 5 mg/L (a) and 50 mg/L (b). Conditions: T = 298 K; ion strength = 0.1 M NaCl.